Coupled Formation of an Amidotransferase Interdomain Ammonia Channel and a Phosphoribosyltransferase Active Site[†,‡]

Joseph M. Krahn,[§] Jeong Hyun Kim,[||,⊥] Mark R. Burns,[#] Ronald J. Parry,[#] Howard Zalkin,[||] and Janet L. Smith*[,§]

Departments of Biological Sciences and Biochemistry, Purdue University, West Lafayette, Indiana 47907, and Department of Chemistry, Rice University, Houston, Texas 77251

Received June 12, 1997; Revised Manuscript Received July 18, 1997[⊗]

ABSTRACT: Activation of glutamine phosphoribosylpyrophosphate (PRPP) amidotransferase (GPATase) by binding of a PRPP substrate analog results in the formation of a 20 Å channel connecting the active site for glutamine hydrolysis in one domain with the PRPP site in a second domain. This solvent-inaccessible channel permits transfer of the NH_3 intermediate between the two active sites. Tunneling of NH_3 may be a common mechanism for glutamine amidotransferase-catalyzed nitrogen transfer and for coordination of catalysis at two distinct active sites in complex enzymes. The 2.4 Å crystal structure of the active conformer of GPATase also provides the first description of an intact active site for the phosphoribosyltransferase (PRTase) family of nucleotide synthesis and salvage enzymes. Chemical assistance to catalysis is provided primarily by the substrate and secondarily by the enzyme in the proposed structure-based mechanism. Different catalytic and inhibitory modes of divalent cation binding to the PRTase active site are revealed in the active conformer of the enzyme and in a feedback-inhibited GMP complex.

Glutamine phosphoribosylpyrophosphate amidotransferase (GPATase)[1] catalyzes the first step of *de novo* purine biosynthesis, transfer of nitrogen from glutamine to phosphoribosylpyrophosphate (PRPP), producing phosphoribosylamine (PRA), pyrophosphate (PP_i), and glutamate. This enzyme belongs to a family of glutamine amidotransferases, which provides the main route for incorporation of nitrogen into biomolecules. The GPATase polypeptide is folded into two structural domains, each belonging to a homologous enzyme family (*1*, *2*). The N-terminal glutamine domain is an Ntn hydrolase with well-understood catalytic functions for conserved enzyme groups (*3*−*6*). The C-terminal acceptor domain is a phosphoribosyltransferase (PRTase), an important family of enzymes for nucleotide salvage and synthesis (*7*). GPATase is a type I PRTase, among two unrelated PRTase families (*8*). Several crystal structures of type I PRTases (*1*, *9*−*14*) have led to the general conclusion that a flexible loop closes the active site upon binding of the unstable substrate PRPP, but none has shown structural details of the enzyme in a catalytically competent, closed conformation. All 16 glutamine amidotransferases possess glutamine and acceptor catalytic domains whose activities are tightly coupled for efficient transfer of nitrogen from glutamine to the acceptor substrate (*15*). The extent to which the two active sites function independently is a major question. Are the two active sites proximal so that essential elements for substrate binding or catalysis are shared, or are they physically separated and catalytically independent with a mechanism for signaling between them? We refer to enzymes with two or more active sites as complex enzymes.

GPATase controls the *de novo* purine biosynthetic pathway through allosteric regulation by feedback inhibitors. Crystal structures of inhibited forms of *Bacillus subtilis* and *Escherichia coli* GPATase have not been informative about the relationship between the two active sites during catalysis (*1*, *6*, *16*, *20*). In each enzyme, the solvent exposed PRTase active site is incompatible with catalysis using a substrate that is spontaneously hydrolyzed. Furthermore, the glutamine and PRTase active sites are separated by approximately 15 Å, much of which is solvent accessible. Two nitrogen transfer mechanisms for the amidotransferases have been discussed for a number of years (*15*, *17*−*19*). Direct transfer of nitrogen from glutamine or activated glutamine to PRPP would require merging of the two active sites into a single "complex" active site. Alternatively, a two-step transfer involving an NH_3 intermediate would require a means to sequester enzyme-bound NH_3 and deliver it to the PRTase active site. For either mechanism, a conformational change relative to the inactive form of the enzyme is required.

Here we present the crystal structure of the closed, active conformer of *E. coli* GPATase containing analogs of substrates glutamine and PRPP in their respective active sites. The structure of the open, inactive form of the enzyme complexed with feedback inhibitor GMP is also presented to illustrate multiple binding modes for divalent metal ions. Structures of the metal-free *E. coli* enzyme have been reported previously (*6*, *16*), as have inhibited forms of the *B. subtilis* enzyme (*1*, *20*).

[†] Supported by NIH Grant GM-26569 and The Robert A. Welch Foundation (C-729) to R.J.P., NIH Grant GM-24658 to H.Z., and NIH Grant DK-42303 to J.L.S.

[‡] Atomic coordinates have been deposited in the Protein Data Bank as lecc for the active conformer and lecb for the GMP-inhibited enzyme.

* To whom correspondence should be addressed.

[§] Department of Biological Sciences, Purdue University.

[||] Department of Biochemistry, Purdue University.

[⊥] Present address: Cellular Oncology R. U., Korea Research Institute of Bioscience and Biotechnology, P.O. Box 115, Yusong, Taejon, 305-600, Korea.

[#] Rice University.

[⊗] Abstract published in *Advance ACS Abstracts,* August 15, 1997.

[1] Abbreviations: DON, 6-diazo-5-oxo-L-*nor*-leucine; GAR, glycinamide ribonucleotide; GPATase, glutamine phosphoribosylpyrophosphate amidotransferase; PEG, poly(ethylene glycol); PP_i, pyrophosphate; PRA, phosphoribosylamine; PRPP, phosphoribosylpyrophosphate; PRTase, phosphoribosyltransferase; cPRPP, 1α-pyrophosphoryl-2α,3α-dihydroxy-4β-cyclopentanemethanol 5-phosphate.

S0006-2960(97)01411-6 CCC: $14.00

Table 1: Summary of Crystal Structure Determinations

	ligands		
	DON, Mn^{2+}-cPRPP	Mg^{2+}-cPRPP	**2**·GMP, Mg^{2+}
space group	$P4_32_12$	$P4_32_12$	$P2_12_12_1$
a (Å)	78.2	80[a]	95.8
b (Å)	78.2	80[a]	113.2
c (Å)	308.8	311[a]	199.6
	Diffraction Data		
data range (Å)	20.0−2.4 (2.5−2.4)	18−3.9 (4.0−3.9)	30.0−2.7 (2.8−2.7)
completeness (%)	88.3 (60.3)	88.2 (54.7)	97.7 (78.9)
R_{sym}[b] (%)	3.6 (17.2)	7.1 (15.1)	9.2 (33.0)
$\langle I/\sigma_I \rangle$	22.7 (3.1)	14.8 (5.3)	12.7 (3.5)
observations (no.)	99285	33875	354923
unique reflections (no.)	35343	8962	58955
	Model Refinement		
working R[c] (%)	17.7		21.9
free R[c] (%)	27.0		29.0
protein atoms (no.)	7758		14904
solvent atoms (no.)	341		235
average *B*-factor (Å^2)	34.2		32.3
rmsd bonded *B*-factors (Å^2)	2.1		5.2
rmsds from target values			
bond lengths (Å)	0.012		0.011
bond angles (deg)	1.9		1.8
torsion angles (deg)	23.0		23.3

[a] Cell dimensions for Mg^{2+}-cPRPP complex crystals were not well determined. [b] $R_{sym} = \sum_h \sum_j |I_h - I_j| / \sum_j I_j$, where I_h = average intensity for all observations of a reflection with unique indices h and $I_j = j$th observation of a reflection with average intensity I_h. [c] $R = \sum |F_o - F_c| / \sum |F_o|$. All measured reflections were included, with the free *R*-factor based on a random 5% subset of the data.

EXPERIMENTAL PROCEDURES

Crystallization and Measurement of Diffraction Data. Crystals of the GPATase Mg^{2+}-cPRPP complexes were grown at 20 °C from solutions of 3.6 mg/mL protein, 0.42 mM cPRPP, 25 mM $MgCl_2$, 40 mM Bis-Tris, pH 5.8, 3.2% 2-propanol, and 7.5% poly(ethylene glycol) (PEG) 3350 by vapor diffusion against a solution of 100 mM Bis-Tris, pH 5.8, 8% 2-propanol, and 15% PEG-3350. Crystals were transferred in two steps to a cryoprotectant solution of 100 mM Bis-Tris, pH 5.8, 10% 2-propanol, 15% PEG 3350, 15% D,L-*meso*-2,3-butanediol, 50 mM $MgCl_2$, and 2 mM cPRPP. Crystals of the Mn^{2+}-cPRPP complex were grown and cryoprotected in the same way as the Mg complex, except for use of DON-inactivated protein (*6*), substitution of $MgCl_2$ by $MnCl_2$ (20 mM in protein solutions), and elimination of PEG 3350. Crystals of the GMP-inhibited complex were grown from solutions of 5 mg/mL protein, 2.5 mM GMP, 10 mM $MgCl_2$, 50 mM Bis-Tris, pH 6.0, 5% PEG 3350, and 5% 2-propanol by vapor diffusion against 100 mM Bis-Tris, pH 6.0, 10% PEG 3350, 10% 2-propanol, and 20 mM $MgCl_2$ and were cryoprotected in reservoir solution with addition of 18% D,L-*meso*-2,3-butanediol and 1 mM GMP. Each data set was obtained from a single crystal, flash frozen to 110 K after 10 min of cryoprotection, using a Rigaku rotating anode Cu Kα source and an R-AXIS IIc image plate system. Images were integrated and scaled with the HKL data processing package (*21*−*22*). Data quality is summarized in Table 1.

Structure Determinations. Phasing for both structures was obtained by molecular replacement from the 2.0 Å model for the inactive form of unliganded GPATase (*16*) using AMORE (*23*). All model refinement was done with X-PLOR (*24*, *25*). Phasing of the $P4_32_12$ active-form structure, which has two subunits in the asymmetric unit, was initiated by positioning each of two single glutaminase domains (249 residues), using data from the Mg^{2+}-cPRPP complex crystal. A crude dimer model was constructed by positioning a PRTase domain core adjacent to each glutaminase domain, as in the inactive form of the enzyme. Multiple-fragment rigid-body refinement resulted in an *R*-factor of 32% (all data, 20.0−3.9 Å). Using the Mn^{2+}-cPRPP data, phases from this model were extended to 3.0 Å by 2-fold averaging and solvent flattening with the AVGSYS programs (*26*). Mn^{2+}-cPRPP and the PRTase flexible loop, not present in the dimer model, were easily interpreted in the resulting electron density map. An anomalous difference map indicated clear peaks for one Mn^{2+} in each PRPP catalytic site and one Mn^{2+} in a crystal lattice contact, explaining the superior diffraction quality of Mn^{2+} cocrystals. Subsequent refinement in X-PLOR and model building in O (*27*) produced the current model. Phasing of the GMP complex was initiated by positioning a GPATase tetramer in the $P2_12_12_1$ unit cell, followed by rigid-body model refinement and phase refinement by 4-fold averaging. The resulting electron density map was easily interpretable for GMP in the allosteric and catalytic sites. Model building and refinement using segmental noncrystallographic symmetry restraints produced the current model. The quality of the models is summarized in Table 1.

RESULTS

Formation of a complex with the stable carbocyclic analog of the substrate PRPP (cPRPP, *28*) was essential to crystallization of the active conformer of GPATase. The highly charged PRTase active site was stabilized in a closed state by binding of a divalent metal ion complex of the charged substrate analog cPRPP. cPRPP is not a substrate for GPATase (*29*), although the Mn^{2+} used for structural work supports catalysis with PRPP (data not shown). Mn^{2+}-cPRPP and Mg^{2+}-cPRPP appear to be identical in structure and in binding to the protein. In the structure of the active

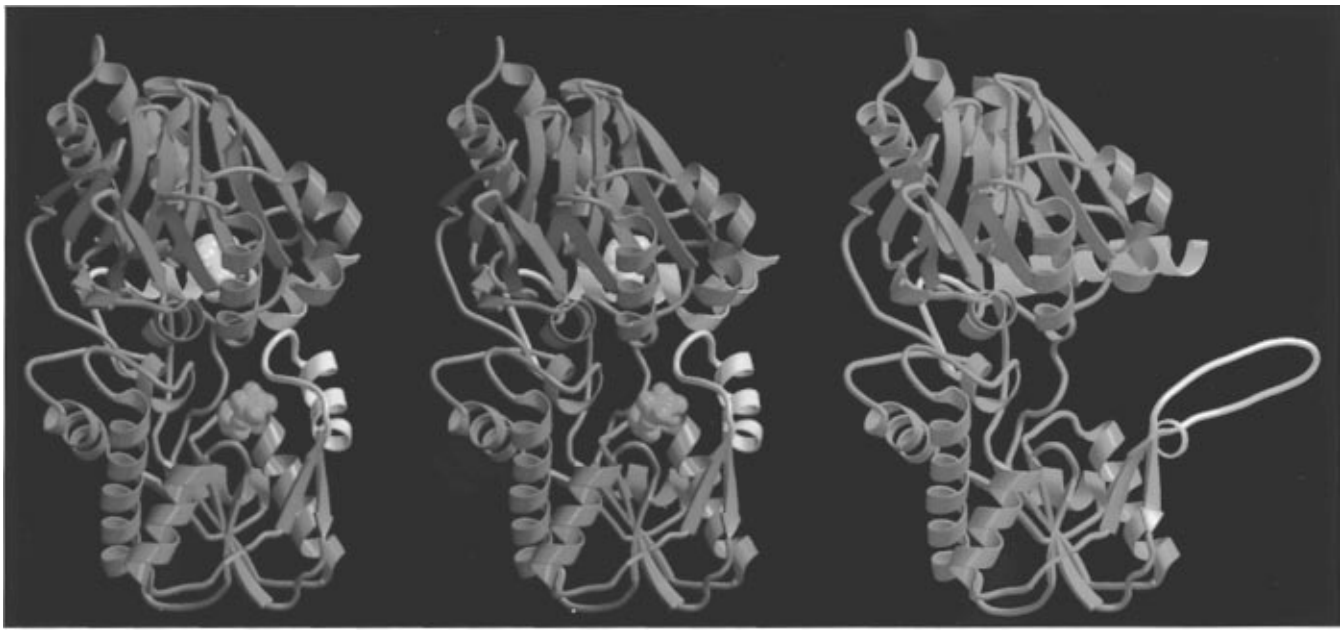

FIGURE 1: Structural change to GPATase upon activation. The purple stereo ribbon diagram is of the GPATase subunit in the active conformation with the glutamine substrate analog DON (yellow) bound to the upper glutamine domain and the PRPP substrate analog cPRPP (red) bound to the lower PRTase domain. The green ribbon diagram depicts the GPATase subunit in the inactive conformation (*16*). Peptides with the most striking structural differences between active and inactive GPATase are highlighted. These are the PRTase flexible loop (residues 325−354) and the C-terminal peptide (residues 471−492).

enzyme conformer, a substrate analog is also bound to the glutamine active site. The glutamine analog 6-diazo-5-oxo-L-*nor*-leucine (DON) was attached covalently to Cys^1, the catalytic nucleophile. Specific contacts of invariant residues with both substrate analogs clearly indicate that this structure is the catalytically active conformer of GPATase. The enzyme structure in complex with the feedback inhibitor GMP represents the inactive form of the enzyme and is virtually identical with previously reported structures (*6*, *16*). The substantial structural differences between active and inactive forms of GPATase occur in loops and extensions to the domain cores.

Formation of the Active Enzyme. The most dramatic structural change in the transition from inactive to active GPATase is an ordering of the PRTase "flexible loop" to cover the analog-bound PRTase active site (Figure 1). This is accompanied by a kinking of the adjacent C-terminal α-helix. These two structural elements together shield the PRTase active site from solvent and sequester cPRPP. The surface area of Mn^{2+}(cPRPP)$(H_2O)_2$ is 100% inaccessible to bulk solvent when bound to the active conformer of the enzyme. The binding cavity created by closure of the PRTase active site is perfectly complementary in shape and charge to the bound Mn^{2+}(cPRPP)$(H_2O)_2$.

Contrary to expectation, total closure of the PRTase active site is achieved with almost no change in the hinge between the glutamine and PRTase domains relative to the inactive form of the enzyme. The two active sites remain well separated, with Cys^1 S_γ and cPRPP C_1 16 Å apart. Thus, essential elements for catalysis and substrate binding are not shared by the two active sites of this complex enzyme. Instead, conserved hydrophobic residues from the interdomain cleft and the ordered PRTase loop create a narrow, solvent-inaccessible channel between active sites. This channel permits diffusion of NH_3 between the two sites through a pathway of conserved residues (Figure 2). Fourteen of the 17 residues along the inferred 20 Å NH_3-transfer route are invariant in the 24 reported GPATase sequences. The channel is formed primarily by loosely packed hydrophobic side chains. Such a structure for intermediate channeling implies that catalysis by the two domains is coordinated by signal transduction.

In GPATase, the signal for activation of catalysis in the glutaminase domain is binding of PRPP to the PRTase domain (*30*). The signal is transduced by three structural changes in the protein. Ordering of the PRTase flexible loop and bending of the C-terminal helix are induced by binding the charged substrate Mg^{+2}-PRPP and result in closure of the PRTase active site. Restructuring of the "glutamine loop", residues 73−79, is a direct steric effect of the first two structural changes (Figure 3). The restructured loop interacts with the glutamine analog DON differently in the active form of the enzyme than in the inactive form. Of particular importance is a salt bridge between the side chain of invariant Arg^{73} and the DON carboxylate, which occurs only in the active conformer of the enzyme. The new conformation of the glutamine loop may be the major contributor to the overall 600-fold PRPP stimulation of glutaminase catalytic efficiency, most of which comes via a 200-fold reduced K_m for glutamine (*6*).

PRTase Active Site. The structure of the active conformer of GPATase provides the first picture of a PRTase active site in a productive complex with a substrate or substrate analog. Mn^{2+}(cPRPP)$(H_2O)_2$ is completely buried within the protein through a total of 21 hydrogen bonds and salt bridges (Figure 4A). This binding mode is remarkable for a molecule as charged as cPRPP but is consistent with the need to protect the reactive substrate PRPP from hydrolysis (*31*) and to prevent protonation of NH_3. The closed active site is a striking contrast to the partially exposed substrate, product, and inhibitor molecules in the structures of open forms of PRTases (*1*, *9*−*12*, *20*, *32*). The active site cavity created by closure of the PRTase loop has a highly charged inner surface perfectly mated to the charges of the bound Mn^{2+}-

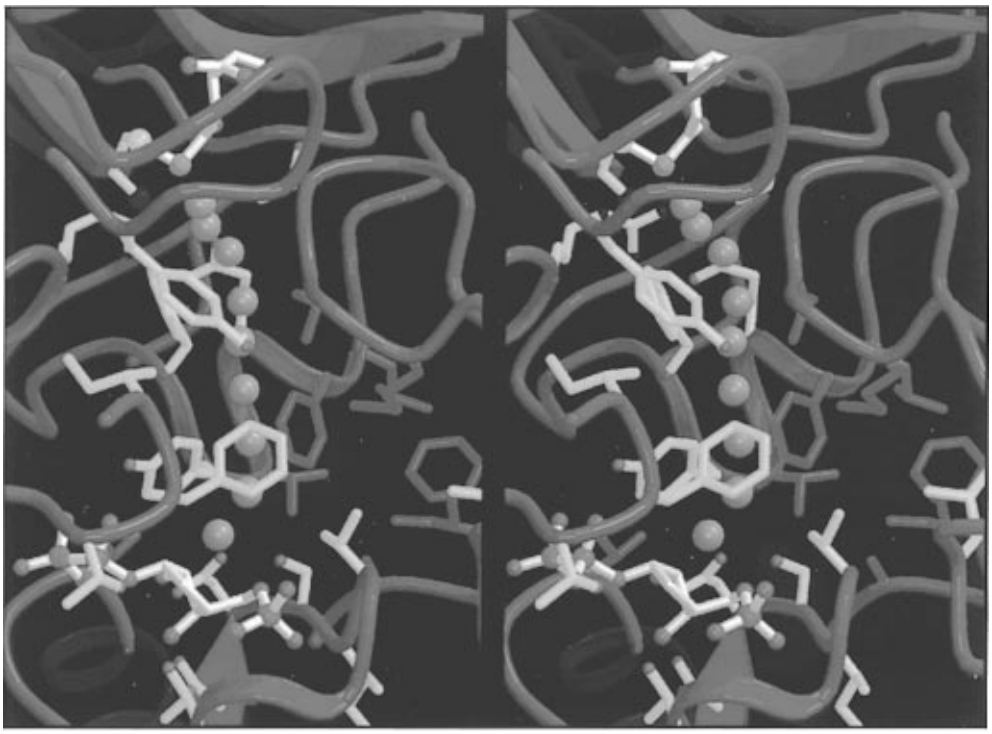

FIGURE 2: NH_3 channel between active sites of GPATase. The stereo diagram shows the glutamine active site at the top and the PRTase active site at the bottom. The proposed pathway of NH_3 is rendered as light blue spheres. Substrate analogs and conserved side chains in the channel are shown explicitly. Heteroatoms are colored by atomic type (O, red; N, blue; S, yellow; P, purple). Substrate analogs are shown with white bonds, invariant side chains lining the channel with yellow bonds (from top to bottom: Cys^{1}, Thr^{76}, Arg^{26}, Glu^{255}, Tyr^{74}, Phe^{259}, Ile^{335}, Phe^{334}, Tyr^{258}, Thr^{333}, Leu^{415}, Asp^{367}, Ser^{368}, Val^{370}, Asp^{366}, Ile^{369}, Thr^{374}), and conservatively substituted side chains with green bonds (from top to bottom: Ile^{407}, Met^{409}, Leu^{253}, Phe^{254}, Val^{257}, Phe^{461}, Ile^{399}, Thr^{309}, Ala^{396}).

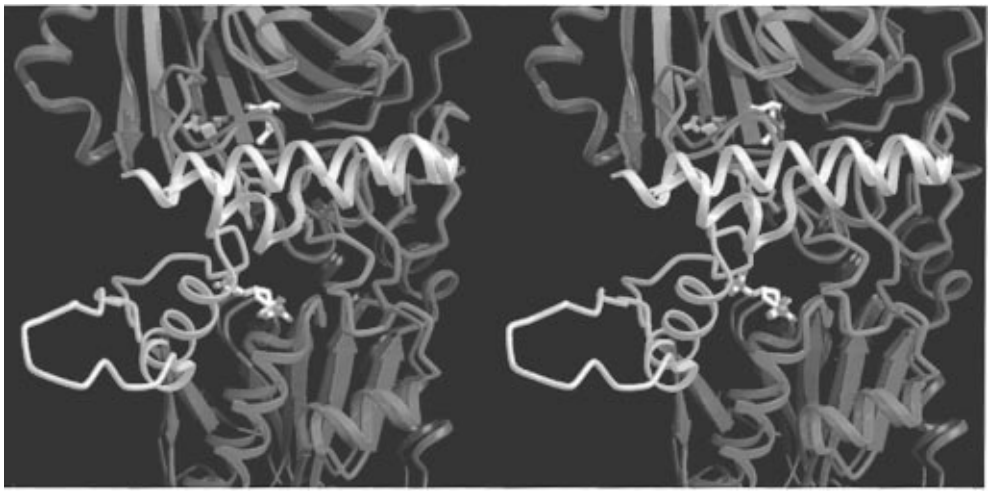

FIGURE 3: Variability in the substrate interaction surface. The stereo diagram is based on superposition of the glutamine domains of active (purple) and inactive (green) conformations of GPATase The highlighted peptides are involved in signal transduction between the PRTase (bottom) and glutamine (top) domains and are the glutamine loop, the C-terminal helix, and the PRTase flexible loop. The substrate analogs DON (top) and cPRPP (bottom) identify the two active sites and are drawn with white bonds (atom coloring as in Figure 2). Side chains of two residues with a demonstrated role in signal transduction (*6*), Arg^{73} and Tyr^{74}, are drawn explicitly for the active and inactive conformations of the enzyme. The 1.5° difference in the interdomain hinge between active and inactive conformations of GPATase is apparent in this view, which is approximately perpendicular to that of Figure 1.

cPRPP complex. Six basic and two acidic side chains line the cavity. Four basic side chains are contributed by the closed PRTase loop, one basic side chain by the loop from another subunit of the tetrameric enzyme, and the remaining charged side chains by the PRPP binding loop (residues 366−374). An unusual *cis* peptide binds Mn^{2+}-cPRPP via hydrogen bonds from the peptide C═O to a Mn^{2+} water ligand and from the peptide NH to the β-phosphate of pyrophosphate (Figure 4B). *cis*-Amides are rare in proteins (*33*), but the *cis*-peptide loop adjacent to the PRPP binding loop is a feature of all GPATase structures and of some other type I PRTases (*6*, *11*, *13*−*14*, *16*, *20*).

Remarkably, GPATase has two modes for binding divalent metal ion. In the closed, active conformer of the enzyme the metal ion binds to ribose pyrophosphate (cyclopentanediol pyrophosphate of the cPRPP analog) and is coordinated by four PRPP oxygens and two water molecules but has no protein ligands (Figure 4B). In the open, inactive form of GPATase complexed with feedback inhibitor GMP, the divalent metal ion is coordinated by both ribose

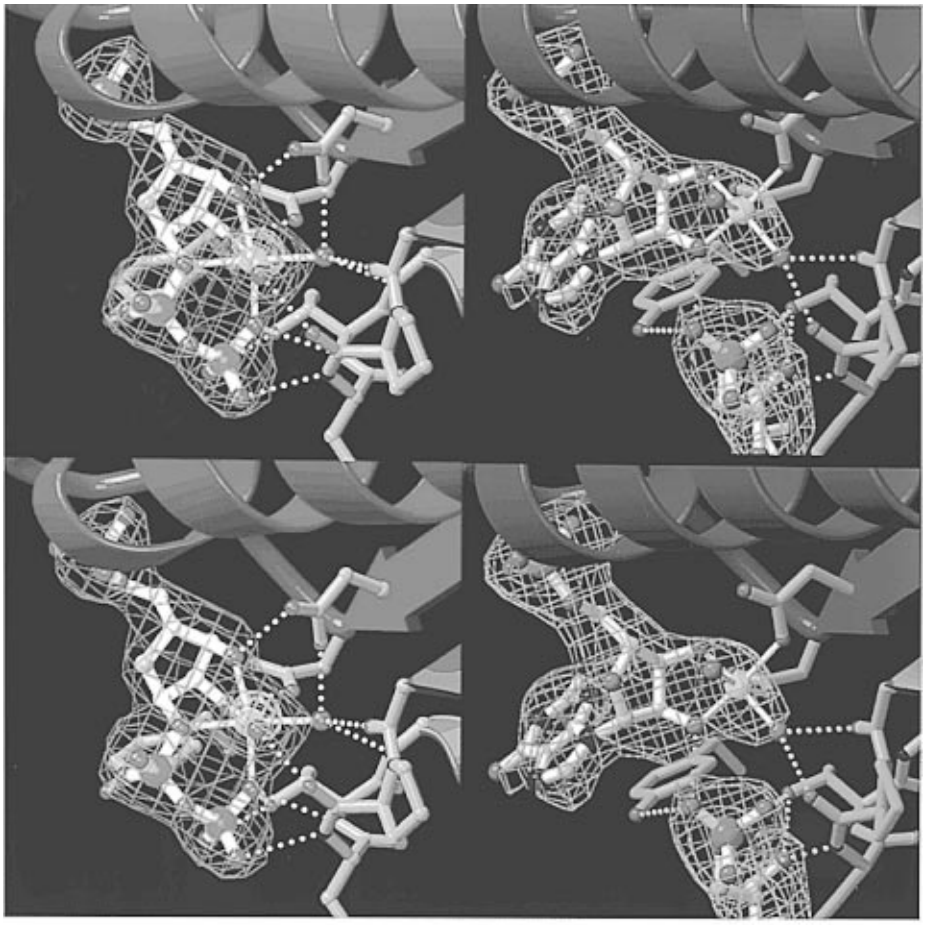

by a pink O_4 atom, which is C in cPRPP. Metal coordination bonds are thin white lines, and hydrogen bonds are dotted lines. (C, bottom right) Product/inhibitor binding mode for the divalent metal ion. Mg^{2+}-GMP is shown bound to the PRPP catalytic site. The two metal sites shown in (B) and (C) overlap and are separated by 1.4 Å, based on superposition of PRPP binding loops. GMP bound to an adjacent "allosteric" site (*1*) is also visible. In this site, the 5′-phosphate of GMP interacts with the same protein groups as the *β*-phosphate of cPRPP in the analog complex, including NH of *cis*-Glu^{303}, OH of Thr^{304}, and OH of Tyr^{258}. Interaction between the two nucleotide sites is also apparent in the hydrogen bond between a phosphate oxygen of GMP in the allosteric site and O_2' of GMP in the catalytic site. Electron density at 2.7 Å resolution, phased with the final model omitting Mg^{2+}-GMP, is shown in blue for $|F_o - F_c|$ coefficients coutoured at 2.5 rms. Atoms are colored as in Figure 2. Coordination and hydrogen bonds are as in (B).

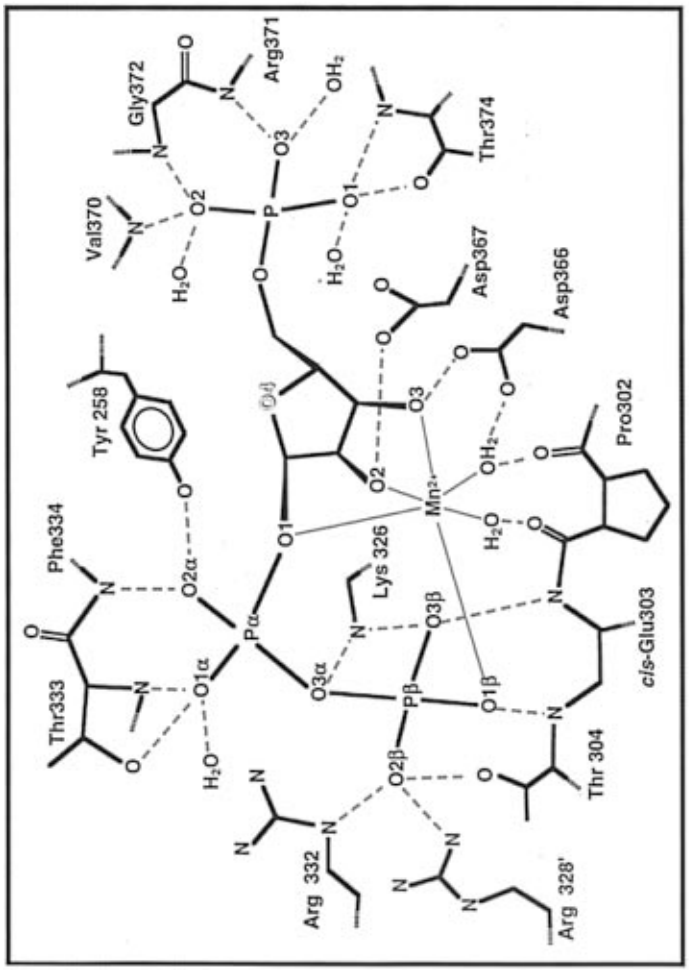

FIGURE 4: The PRTase active site of GPATase. (A, left) Interactions of substrate analog cPRPP. Hydrogen bonds are drawn as dashed lines, and coordination bonds to Mn^{2+} are thin solid lines. The PRTase active site cavity includes three additional charged side chains that do not contact cPRPP directly and are not shown in this schematic diagram: Arg^{342} and Lys^{349} from the PRTase loop and Arg^{371} from the PRPP binding loop. The analog is drawn in black; groups from the primary protein subunit are in blue and from the secondary subunit in green. The chemical difference between PRPP and its analog is shown with outline lettering for O_4, which is C in cPRPP. (B, top right) Catalytic binding mode for the divalent metal ion in the PRTase active site. Mn^{2+}-cPRPP is shown with hydrogen bonds to the PRPP binding loop. Electron density at 2.4 Å resolution, phased with the final model omitting Mn^{2+}-cPRPP, is shown in blue for $|F_o - F_c|$ coefficients coutoured at 2.5 rms and in pink for $|F^+ - F^-|$ contoured at 7 rms. Atoms are colored as in Figure 2. The chemical difference between PRPP and its analog cPRPP is illustrated

hydroxyls, by the dual carboxylate side chains of Asp^{366} and Asp^{367}, and by two water molecules (Figure 4C). Thus the common structure of divalent metal ion coordinated to ribose 2- and 3-hydroxyl groups binds to the enzyme in two different orientations, dependent on the presence of α1-pyrophosphate. Metal ligation appears to be the primary determinant of the conformation of bound analog or substrate. C_3-*exo* ring pucker best fits both the electron density for cPRPP and the constraint of metal ligation by all three exocyclic oxygen atoms. The pyrophosphate tail is curled back toward the ring due to metal ligation by a terminal oxygen and by the O_1 bridging oxygen.

DISCUSSION

Intermediate Channeling. Formation of a channel for the NH_3 intermediate was an unanticipated result of the current work. A hydrophobic channel is ideal for transfer of NH_3 because it excludes water during formation, prevents the protonation of ammonia, and includes no hydrogen-bonding groups, which might hinder diffusion of NH_3 en route to the acceptor substrate PRPP. The NH_3 channel discriminates between mechanisms for nitrogen transfer by GPATase and other glutamine amidotransferases. The structure of the active conformer of GPATase is consistent with mechanisms involving formation of a free NH_3 intermediate but would seem to rule out mechanisms involving direct transfer of nitrogen from glutamine or an activated form of glutamine to the acceptor substrate. The only well-characterized structural example of intermediate channeling inside a protein is tryptophan synthase (*34*, *35*), which channels indole between two catalytic sites. Tryptophan synthase has other features in common with GPATase including communication between the two active sites to couple the half-reactions and complete shielding of both active sites from bulk solvent.

Creation of an NH_3 tunnel is an elegantly simple means to carry out nitrogen transfer from glutamine to PRPP. We propose that other amidotransferases also employ the same scheme for coupling their glutamine and acceptor domains because it is a simple solution to the problem of catalysis in complex enzymes. Each amidotransferase contains a glutamine domain from one of two homologous families (*15*) and an acceptor domain, which also may belong to a homologous enzyme family. Catalytic activities of the two active sites are coupled by signal transduction and not by merger into a single active site. In retrospect, fine tuning an existing catalytic domain for optimal activity, depending on availability of substrates or inhibitors, seems a far simpler task in molecular design than is merger of two precise active sites into one.[2]

PRTase Catalysis. Binding of substrate analog clearly drives formation of the closed PRTase active site, which, with six basic and two acidic side chains, will not form in the absence of a suitable ligand. The closed active site must therefore be regarded as a transient form of the enzyme. In previously reported crystal structures of type I PRTases, a variety of flexible loop conformations was observed, all poorly ordered and none closed. Subunit interfaces also vary, such that the flexible loop apparently closes over the active site of a second subunit of orotate PRTase (*13*, *36*). Ordering of the flexible loop into the active site during catalysis is predicted in nearly all the earlier structural reports of type I PRTases and has ample precedent in structural enzymology. Total burial of the substrate was not anticipated, although it is consistent with the need to exclude water from the catalytic reaction. We predict that other type I PRTases will also bury $Mg^{2+}(PRPP)(H_2O)_2$ during catalysis.

No catalytic residues are obvious in the closed PRTase active site of GPATase. Instead, the unstable, "activated" substrate appears to assist catalysis directly, with the enzyme playing a secondary catalytic role. We propose that the enzyme guides catalysis by binding PRPP in an orientation that favors breakdown to products and by sequestering the active site so that PP_i is displaced by NH_3 and not by water. Accordingly, the β face of the ribose ring is directed toward the NH_3 channel so that any nucleophile in the channel will attack PRPP at C_1 (Figure 2). The hydrophobic surface of the channel excludes water and ensures that NH_3 produced in the glutamine domain is the only nucleophile to enter the channel.

Substrate-assisted catalysis by type I PRTases is proposed on the basis of analysis of analog binding to the PRTase active site of GPATase. Substrate assistance functions at two levels. The substrate conformation is fixed to promote in-line attack at C_1, and formal charges on the substrate are exploited to form and to stabilize transient positive charge. The metal ion, which has no protein ligands, is a major contributor to both of these effects. It fixes analog conformation via four coordination bonds, which determine both the pucker of the ring and the conformation of the pyrophosphate tail (Figure 4B). The structure of the cPRPP complex is consistent with an anticipated oxycarbonium ion catalytic intermediate (*37*−*39*). The electron-withdrawing power of the metal ion promotes formation of the oxycarbonium ion, which is stabilized by the negatively charged pyrophosphate tail. Two details of cPRPP conformation also support catalysis. The C_3-*exo* ring pucker fixes the bond opposite C_3 in a nearly eclipsed conformation, which promotes formation of planar geometry at C_1 and partial double bond character in the C_1-O_4 bond of the oxycarbonium ion intermediate. An α-phosphate oxygen of the pyrophosphate tail ($O_{2\alpha}$) points toward the C_1 atom. This conformation is optimal for formation of a CH−O interaction between the pyrophosphate $O_{2\alpha}$ and the C_1 proton to stabilize planar geometry at C_1 and to provide electrostatic stabilization for an oxycarbonium ion. The dual carboxylate side chains of invariant residues Asp^{366} and Asp^{367} may provide additional stabilization to the oxycarbonium ion via hydrogen bonds to the ribose hydroxyls. The pair of acidic side chains is a hallmark of the PRPP binding loop of type I PRTases. The hydroxyl of Tyr^{258} may be a proton shuttle between the attacking NH_3 and the leaving PP_i, although direct proton transfer may also occur. Although our structure-based mechanism invokes PRPP-facilitated catalysis, specific roles for enzyme side chains, not presently apparent, remain possible and should be addressed in future biochemical experiments.

The structures of substrate analog and inhibitor complexes of GPATase reveal two overlapping Mg^{2+} sites that share four of six ligands, consistent with kinetic analyses of *B. subtilis* GPATase that suggested the presence of two metal sites (*40*). Metal ligation to the pyrophosphate tail in the closed, active conformer of GPATase is similar to that

[2] Channels have been described recently for intermediates in the multistep reaction catalyzed by carbamoyl phosphate synthetase (*43*).

reported in the open, Mg^{2+}-PRPP complex of orotate PRTase (*32*). The noncatalytic metal binding mode has also been observed in other nucleotide complexes of GPATase and in product complexes of other PRTases (*12, 20*). The two modes of metal binding reflect the variety of orientations observed for substrate, analog, products, and inhibitors in the type I PRTase active site. The importance of ligand, either cPRPP or GMP, to metal binding in GPATase supports the idea that the protein binds a metal−ligand complex and not the metal alone (*41*). The features of substrate binding to GPATase described above are compatible with available biochemical, sequence, and structural data for other type I PRTases. Thus, the conclusions about substrate-assisted catalysis and active site closure are expected to apply to all members of the predominant type I PRTase family.

Substrate Binding and Product Release. Two important aspects of GPATase catalysis, accessibility of the glutaminase active site to substrate glutamine and release of product PRA from the PRTase active site, remain unexplained in light of the structure of the active conformer of the enzyme. The glutaminase active site is closed to bulk solvent in every one of 16 different crystal environments for the GPATase subunit, active or inactive, analog-bound, or empty (*1, 6, 16, 20*). Although this is a simple means for the enzyme to prevent indiscriminate glutamine hydrolysis in absence of the acceptor substrate PRPP, it is not apparent how glutamine gains access to the site nor how glutamate is released. The second enigma of GPATase catalysis is the fate of the extremely labile product PRA. Given its chemical instability, how is PRA protected against hydrolysis? Product channeling from GPATase to glycinamide ribonucleotide (GAR) synthetase, the next enzyme of the purine biosynthetic pathway, has indirect experimental support, but the two enzymes do not form a stable complex (*42*). Answers to both questions may lie in the structural variability of GPATase demonstrated in this work. In normal turnover of PRTases, the closed, active form is associated only with PRPP binding, while the open, inactive form predominates in the resting enzyme. This is consistent with observation of the open form in all PRTase crystal structures preceding the current work and with the highly charged inner surface of the closed PRTase active site cavity. In GPATase, the PRTase active site is closed by coupled structural changes in the conserved PRTase loop and the highly variable C-terminal peptide. The C-terminal peptide and the glutamine loop (residues 73−79) contribute to closure of the glutaminase active site differently in the active and inactive forms of the enzyme. These three flexible structures—the PRTase loop, the C-terminal peptide, and the glutamine loop—converge on a surface of the enzyme that is the likeliest site of glutamine access and PRA release (Figure 3). Binding of glutamine and release of PRA both may be associated with conformations intermediate between the observed active and inactive "end points" of GPATase structural variability. In this model the PRTase loop and C-terminal peptide together form a surface for interaction with GAR synthetase, and the glutamine loop and C-terminal peptide flex to open the glutaminase active site.

Relationship to Carbamoyl Phosphate Synthetase. After completion of this work and this paper, a report appeared describing the crystal structure of *E. coli* carbamoyl phosphate synthetase and a channel connecting sites for glutamine, carboxy phosphate, and carbamate (*43*). These results confirm our prediction (*2*) of a universal amidotransferase NH_3 channel for nitrogen transfer between glutamine and acceptor sites. GPATase and carbamoyl phosphate synthetase belong to the Ntn and Triad amidotransferase families (*2*), respectively, and have unrelated glutaminase domains. The NH_3 channels of GPATase and carbamoyl phosphate synthetase differ substantially in polarity, although both enzymes must exclude water from reaction with the labile acceptor substrates PRPP and carboxy phosphate. This apparent discrepancy is consistent with the rather different structural biology of GPATase and carbamoyl phosphate synthetase. A hydrophobic NH_3 channel is formed during one step of the catalytic cycle of GPATase by amino acids that are otherwise exposed to bulk solvent. Such a channel could not exclude water effectively if it were polar. In contrast, the polar groups forming the NH_3 channel of carbamoyl phosphate synthetase appear to be permanently inside the enzyme and must employ another mechanism for water exclusion.

REFERENCES

1. Smith, J. L., Zaluzec, E. J., Wery, J.-P., Niu, L., Switzer, R. L., Zalkin, H., and Satow, Y. (1994) *Science 264*, 1427−1433.
2. Zalkin, H., and Smith, J. L. (1997) *Adv. Enzymol. Relat. Areas Mol. Biol.* (in press).
3. Brannigan, J. A., Dodson, G., Duggleby, H. J., Moody, P. C. E., Smith, J. L., Tomchick, D. R., and Murzin, A. G. (1995) *Nature 378*, 416−419.
4. Smith, J. L. (1995) *Biochem. Soc. Trans. 23*, 894−898.
5. Isupov, M. N., Obmolova, G., Butterworth, S., Badet-Denisot, M.-A., Badet, B., Polikarpov, I., Littlechild, J. A., and Teplyakov, A. (1996) *Structure 4*, 801−810.
6. Kim, J. H., Krahn, J. M., Tomchick, D. R., Smith, J. L., and Zalkin, H. (1996) *J. Biol. Chem. 271*, 15549−15557.
7. Musick, W. D. L. (1981) *CRC Crit. Rev. Biochem. 11*, 1.
8. Eads, J. C., Ozturk, D., Wexler, T. B., Grubmeyer, C., and Sacchettini, J. C. (1997) *Structure 5*, 47−58.
9. Scapin, G., Grubmeyer, C., and Sacchettini, J. C. (1994) *Biochemistry 33*, 1287−1294.
10. Eads, J. C., Scapin, G., Xu, Y., Grubmeyer, C., and Sacchettini, J. C. (1994) *Cell 78*, 325−334.
11. Somoza, J. R., Chin, M. S., Focia, P. J., Wang, C. C., and Fletterick, R. J. (1996) *Biochemistry 35*, 7032−7040.
12. Schumacher, M. A., Carter, D., Roos, D. S., Ullman, B., and Brennan, R. G. (1996) *Nat. Struct. Biol. 3*, 881−887.
13. Henriksen, A., Aghajari, N., Jensen, K. F., and Gajhede, M. (1996) *Biochemistry 35*, 3803−3809.
14. Vos, S., de Jersey, J., and Martin, J. L. (1997) *Biochemistry 36*, 4125−4134.
15. Zalkin, H. (1993) *Adv. Enzymol. Relat. Areas Mol. Biol. 66*, 203−309.
16. Muchmore, C. R. A., Krahn, J. M., Kim, J. H., Zalkin, H., and Smith, J. L. (1997) *Protein Sci.* (in press).
17. Wyngaarden, J. B. (1972) *Curr. Top. Cell. Regul. 5*, 135−176.
18. Buchanan, J. M. (1973) *Adv. Enzymol. Relat. Areas Mol. Biol. 39*, 91−183.
19. Stoker, P. W., O'Leary, M. H., Boehlein, S. K., Schuster, S. M., and Richards, N. G. J. (1996) *Biochemistry 35*, 3024−3030.
20. Chen, S., Tomchick, D. R., Wolle, D., Hu, P., Smith, J. L., Switzer, R. L., and Zalkin, H. (1997) *Biochemistry 36*, 10718−10726.
21. Otwinowski, Z., and Minor, W. (1997) *Methods Enzymol. 276*, 307−326.
22. Otwinowski, Z. (1993) in *Data Collection and Processing, Proceedings of the CCP4 Study Weekend, 29−30 January 1993* (Sawyer, L., Isaacs, N., and Bailey, S., Compilers) pp 56−62, SERC Laboratory, Daresbury, Warrington, England.
23. Navaza, J., and Saludjian, P. (1997) *Methods Enzymol. 276*, 581−594.

24. Brünger, A. T. (1992) *X-PLOR Version 3.1, A System for X-ray Crystallography and NMR*, 382 pp, Yale University Press, New Haven and London.
25. Brünger, A. T., Krukowski, A., and Erickson, J. W. (1990) *Acta Crystallogr. A46*, 585−593.
26. Bolin, J. T., Smith, J. L., and Muchmore, S. W. (1993) *Abstracts of the American Crystallographic Association*, 51.
27. Jones, T. A., Zou, J.-Y., Cowan, S. W., and Kjeldgaard, M. (1991) *Acta Crystallogr. A47*, 110−119.
28. Parry, R. J., Burns, M. R., Jiralerspong, S., and Alemany, L. (1997) *Tetrahedron 53*, 7077−7088.
29. Kim, J. H., Wolle, D., Haridas, K., Parry, R. J., Smith, J. L., and Zalkin, H. (1995) *J. Biol. Chem. 270*, 17394−17399.
30. Messenger, L. J., and Zalkin, H. (1979) *J. Biol. Chem. 254*, 3382−3392.
31. McClard, R. W., Fischer, A. C., Mauldin, S. K., and Jones, M. E. (1984) *Bioorg. Chem. 12*, 339−348.
32. Scapin, G., Ozturk, D. H., Grubmeyer, C., and Sacchettini, J. C. (1995) *Biochemistry 34*, 10744−10754.
33. Herzberg, O., and Moult, J. (1991) *Proteins: Struct., Funct., Genet. 11*, 223−229.
34. Hyde, C. C., Ahmed, S. A., Padlan, E. A., Miles, E. W., and Davies, D. R. (1988) *J. Biol. Chem. 263*, 17857−17871.
35. Rhee, S., Parris, K. D., Ahmed, S. A., Miles, E. W., and Davies, D. R. (1996) *Biochemistry 35*, 4211−4221.
36. Ozturk, D. H., Dorfman, R. H., Scapin, G., Sacchettini, J. C., and Grubmeyer, C. (1995) *Biochemistry 34*, 10764−10770.
37. Goitein, R. K., Chelsky, D., and Parsons, S. M. (1978) *J. Biol. Chem. 253*, 2963−2971.
38. Bhatia, M. B., Vinitsky, A., and Grubmeyer, C. (1990) *Biochemistry 29*, 10480−10487.
39. Tao, W., Grubmeyer, C., and Blanchard, J. S. (1996) *Biochemistry 35*, 14−21.
40. Meyer, E., and Switzer, R. L. (1979) *J. Biol. Chem. 254*, 5397−5402.
41. Bhatia, M. B., and Grubmeyer, C. (1993) *Arch. Biochem. Biophys. 303*, 321−325.
42. Rudolph, J., and Stubbe, J. (1995) *Biochemistry 34*, 2241−2250.
43. Thoden, J. B., Holden, H. M., Wesenberg, G., Raushel, F. M., and Rayment, I. (1997) *Biochemistry 36*, 6305−6316.

BI9714114